VNU Journal of Science: Mathematics - Physics

Journal homepage: https://js.vnu.edu.vn/MaP

Original Article

Enhanced Microwave Absorption Properties of $SrFe_{12}O_{19}/CoFe_2O_4$ Hard–Soft Ferrite Composites

Tran Thi Viet Nga[1,*], Dinh Thi Tho[2], Do Xuan Tung[2], Nguyen Pham Yen Nhi[1], Nguyen Van Duy[1]

[1]*School of Materials Science and Engineering, Hanoi University of Science and Technology, 1, Dai Co Viet, Hanoi, Vietnam*

[2]*Faculty of Engineering Physics, Hanoi University of Science and Technology, 1 Dai Co Viet, Hanoi, Vietnam*

Received 21st May 2026
Revised 30th June 2026; Accepted 31st July 2026

Abstract: Electromagnetic (EM) wave pollution has become a severe problem in the civilian and military sectors because of the increasingly popular in Mobile communications, the Internet, and digital data networks. EM wave pollution not only threatens information security but also induces various human diseases. This work presents a comparative investigation of the electromagnetic wave absorption performance of $SrFe_{12}O_{19}$, $CoFe_2O_4$, and $SrFe_{12}O_{19}/CoFe_2O_4$ materials. The samples were synthesized using a sol–gel method combined with thermal annealing treatment. X-ray diffractometry (XRD), scanning electron microscopy (SEM), vibrating sample magnetometer (VSM) and vector network analysis (VNA) are achieved for microstructural, magnetic and electromagnetic characterization of the sample. The results indicate that the nanocomposite exhibits enhanced electromagnetic wave absorption properties compared with the individual $SrFe_{12}O_{19}$ and $CoFe_2O_4$ nanomaterials. The composite sample achieved a minimum reflection loss of −43.3 dB at 17 GHz with a thickness of 3 mm. The $SrFe_{12}O_{19}$/ $CoFe_2O_4$ nanocomposite exhibited superior performance in terms of both minimum reflection loss and effective absorption bandwidth, indicating its promising potential for microwave absorption applications.

Keywords: $SrFe_{12}O_{19}/CoFe_2O_4$, composite materials, microwave absorption.

* Corresponding author.
*E-mail address:*nga.tranthiviet@hust.edu.vn

https//doi.org/10.25073/2588-1124/vnumap.5149

1. Introduction

The rapid development of wireless communication systems, high-frequency electronic devices, and radar technologies has led to increasing electromagnetic (EM) pollution, which can cause serious electromagnetic interference and threaten the stability and reliability of electronic systems [1, 2]. Therefore, the development of high-performance electromagnetic wave absorbing materials with lightweight characteristics, strong absorption capability, broad effective absorption bandwidth, and excellent environmental stability has attracted considerable attention in recent years [3, 4]. Among various microwave absorbing materials, magnetic ferrites have been widely investigated because of their high magnetic permeability, excellent chemical stability, corrosion resistance, and tunable electromagnetic properties [5, 6]. In particular, M-type strontium hexaferrite $SrFe_{12}O_{19}$ is considered a promising candidate for microwave absorption applications due to its high magnetocrystalline anisotropy, large coercivity, good thermal stability, and strong magnetic loss behavior in the GHz frequency range [7]. However, the high anisotropy field and relatively low dielectric loss of pure $SrFe_{12}O_{19}$ often result in poor impedance matching, limiting its microwave absorption performance [8, 9].

To overcome these limitations, the construction of composite structures combining hard magnetic and soft magnetic ferrites has emerged as an effective strategy to enhance electromagnetic wave absorption properties [6, 10, 11]. Spinel cobalt ferrite $CoFe_2O_4$ is a typical soft magnetic material possessing high saturation magnetization, moderate coercivity, high electrical resistivity, and significant magnetic loss capability [6]. The incorporation of $CoFe_2O_4$ into $SrFe_{12}O_{19}$ can effectively improve impedance matching, interfacial polarization, and synergistic dielectric–magnetic loss mechanisms. Furthermore, the exchange coupling interaction between hard and soft magnetic phases can contribute to enhanced magnetic resonance behavior and attenuation capability of electromagnetic waves [12].

Recently, several studies have demonstrated that hexaferrite/spinel ferrite composites exhibit superior microwave absorption performance compared to single-phase ferrites [13-16]. The enhancement is mainly attributed to the optimized electromagnetic parameters, multiple relaxation processes, interfacial polarization, and improved attenuation characteristics generated at the heterogeneous interfaces. In particular, $SrFe_{12}O_{19}/CoFe_2O_4$ composites are expected to exhibit strong microwave attenuation owing to the synergistic combination of the high anisotropy field of $SrFe_{12}O_{19}$ and the excellent soft magnetic behavior of $CoFe_2O_4$ [14]. Nevertheless, the relationship between composite composition, microstructure, magnetic properties, and electromagnetic wave absorption performance still requires further investigation.

In this work, $SrFe_{12}O_{19}$, $CoFe_2O_4$ and $SrFe_{12}O_{19}$/ $CoFe_2O_4$ composite materials were synthesized and systematically investigated. The phase structure, morphology, magnetic properties, and electromagnetic wave absorption characteristics of the composites were analyzed in detail. The reflection loss and effective absorption bandwidth in the GHz frequency range were evaluated to compare the microwave absorption performance of the $SrFe_{12}O_{19}/CoFe_2O_4$ (1:5) composite with those of the individual ferrite components. The obtained results provide valuable insights into the design of high-efficiency ferrite-based electromagnetic wave absorbing materials for practical applications in electromagnetic interference shielding and microwave attenuation technologies.

2. Experiments

$SrFe_{12}O_{19}$ and $CoFe_2O_4$ nanopowders were synthesized by via sol-gel method. $Fe(NO_3)_3$. $9H_2O$, $Sr(NO_3)_2$ and $Co(NO_3)_2.6H_2O$ were dissolved in deionized water to form an aqueous solution of 1M. The nitrates used to synthesize $SrFe_{12}O_{19}$ and $CoFe_2O_4$ were dissolved in deionized water with the molar ratio Sr/Fe is 1/11.5 and Co/Fe is 1/2. Citric acid (AC) was then added into the solution at fixed [Sr^{2+} +

Fe^{3+}] : AC and [Co^{2+} + Fe+] : AC molar ratio of 1:3. NH_4OH was used to adjust the pH to 1. After the pH had been stabilized, the solution was stirred at 1000 rpm and gradually evaporated at 80°C. As the water evaporated, the remainder became highly viscous gels as a result of the chelation process. These gels were dried at 110°C for 24 h, and then heated at 450°C (for $SrFe_{12}O_{19}$) and 200ºC (for $CoFe_2O_4$) for 2 hours to eliminate the remaining residual water and other organic impurities (aerogels were formed). To form the hexaferrite and spinel phase, the gels were calcined in air at 900°C for 2 hours. $SrFe_{12}O_{19}/CoFe_2O_4$ nanopowder (R_m) was synthesized using the aerogel powders obtained previously. $SrFe_{12}O_{19}$ and $CoFe_2O_4$ aerogel powders were uniformly mixed with mass ratios (R_m) of 1:5, denoted as R_m15. Then the mixtures were pressed into platelets of 6 mm in diameter and sintered at 900ºC for 2 hours. The crystal structure and phases of the obtained samples were identified via X-ray powder diffraction (XRD) using a Siemens D5000 diffractometer (CuKα radiation, λ = 1.54056 Å). Morphological features and particle size were observed by scanning electron microscopy (SEM, JEOL-JSM 7600F). The magnetic were measured using a vibrating sample magnetometer (VSM, Lakeshore 7410) with applied magnetic fields up to 15 kOe.

In this study, $SrFe_{12}O_{19}/CoFe_2O_4$ nanoparticles (R_m) combined with paraffin have a mass concentration of 30%, displaying promising blending characteristics. Upon undergoing toroidal molding, the mixtures acquired an internal diameter of 3.04 mm and an external diameter of 7.00 mm. The microwave absorption properties were determined using the Keysight PNA-X N5242A vector network analyzer.

3. Results and Discussion

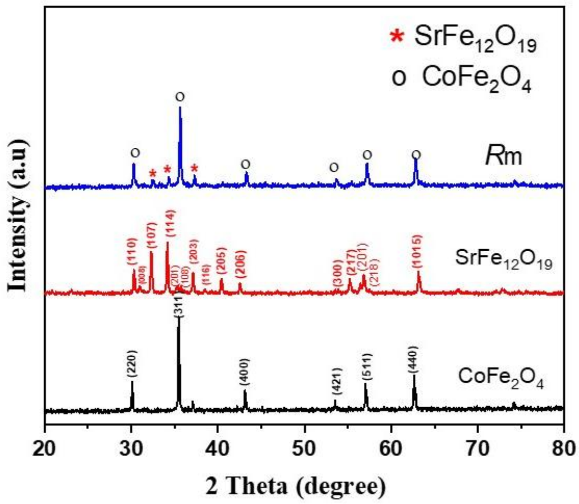

Figure 1. XRD patterns of $SrFe_{12}O_{19}$, $CoFe_2O_4$ and R_m samples.

Figure 1 show the XRD parterns of samples. For $SrFe_{12}O_{19}$, the samples were observed to form a single phase after calcination at 900 °C for 2 h. The diffraction peaks are sharp and intense, indicating a hexagonal crystal structure with the space group $P6_3/mmc$. The characteristic diffraction peaks of $SrFe_{12}O_{19}$ phase located at 2θ = 30.1°, 32.7°, 34.3°, 35.5°, 37.4°, 40.1°, 42.4°, 55.7°, 57.0°, and 63.3° correspond to the crystallographic planes of (110), (107), (114), (200), (203), (205), (206), (217), (20 11), and (220), respectively [17], which are consistent with the standard PDF card No. 00-033-1340. No impurity peaks were observed in the XRD pattern, confirming that $SrFe_{12}O_{19}$ is the dominant phase in the sample. Similarly, the $CoFe_2O_4$ sample exhibits a cubic crystal structure with a spinel-type configuration. The characteristic diffraction peaks appearing at 2θ values of 30.4°, 35.5°, 37.2°, 43.1°, 53.8°, 57.1°, 63.0°, and 74.4° are indexed to the (220), (311), (222), (400), (422), (511), (440), and (533) crystallographic planes, respectively, in agreement with the standard PDF card No. 00-220-1086. The sharp and intense diffraction peaks indicate that the sample possesses a well-crystallized spinel structure with high phase purity and good crystallinity. Meanwhile, both $CoFe_2O_4$ and $SrFe_{12}O_{19}$ phases coexist in the R_m sample.

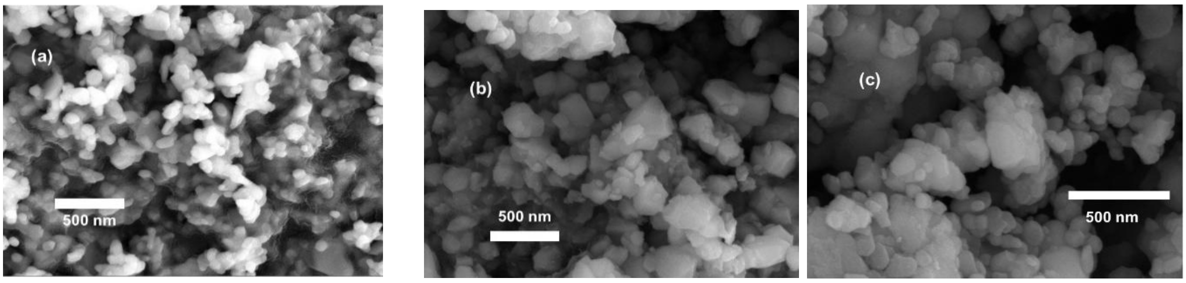

Figure 2. SEM micrographs of $SrFe_{12}O_{19}$ (a), $CoFe_2O_4$ (b) and R_m (c) samples.

From the SEM images of the samples (Figure 2), it can be observed that the $SrFe_{12}O_{19}$ sample consists of hexagonal-shaped particles with an average particle size ranging from 50 to 100 nm. The $CoFe_2O_4$ sample is composed of tetrahedral-like particles with non-uniform particle sizes distributed in the range of 50–200 nm. Meanwhile, the R_m sample is composed of hexagonal and cubic particles with similar sizes, which are homogeneously interspersed throughout the composite.

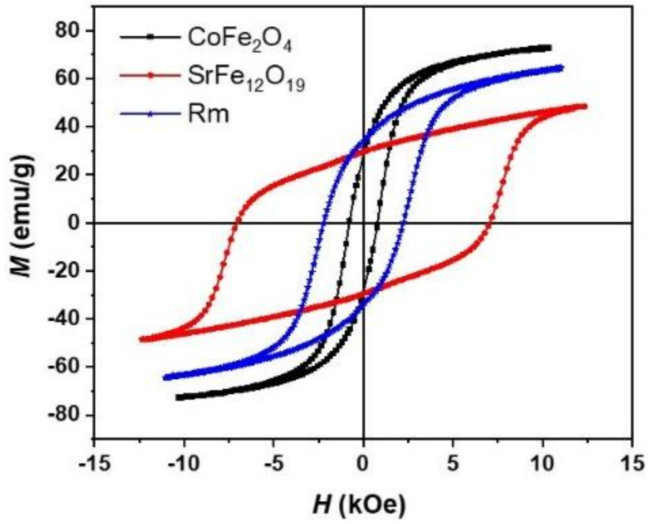

Figure 3. Hysteresis loops of $SrFe_{12}O_{19}$, $CoFe_2O_4$ and R_m samples.

Figure 3 a compares the hysteresis loops of the three samples at room temperature. The $SrFe_{12}O_{19}$ sample exhibits a complex magnetic behavior, with coercivity H_C and saturation magnetization M_S reaching 7.1 kOe and 48.6 emu/g, respectively. The coercivity value of the $SrFe_{12}O_{19}$ sample obtained in this work is approximately equal to that reported for samples synthesized by the same sol–gel method under similar processing conditions in previous studies [18]. However, the magnetization values obtained in this study are about 23% lower than those reported previously, which can likely be explained by the poorer particle size uniformity of the synthesized samples. The hysteresis loops of the R_m sample show single- step hysteresis loops suggesting two magnetic phase are exchange coupled to each other [16]. The MS and HC of the Rm sample reachs 64 emu/g and 2.2 kOe, respectively. The HC of Rm sample is larger about 20% than that of $CoFe_2O_4$ sample and lower about 70% than that of $SrFe_{12}O_{19}$ sample. Meanwhile, the MS of Rm sample is larger about 30% than that of SrFe12O19 sample and lower about 12% than that of $CoFe_2O_4$ sample. This result was mainly attributed to the MS of $CoFe_2O_4$ is higher than that of $SrFe_{12}O_{19}$ and the exchange coupled to each other in Rm sample.

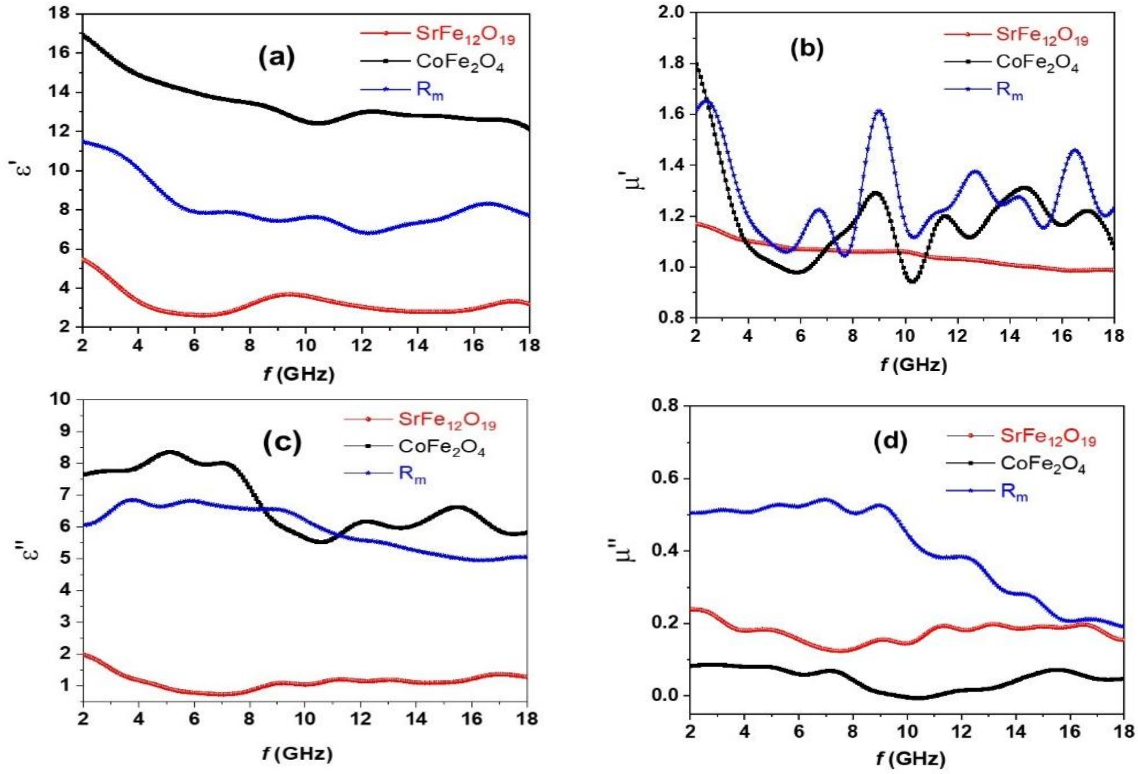

Figure 4. Frequency dependence of the real (a, b) and imaginary (c, d) parts of complex permittivity (ε) and complex permeability (μ), respectively.

Figure 4 shows the frequency dependence of the real (ε') and imaginary (ε'') parts of the complex permittivity, as well as the real (μ') and imaginary (μ'') parts of the complex permeability, for $SrFe_{12}O_{19}$, $CoFe_2O_4$, and the $R_m$composite samples in the frequency range of 2–18 GHz. In general, both $\varepsilon'$and ε''slightly decrease with increasing frequency, which is consistent with dielectric relaxation behavior and the Maxwell–Wagner interfacial polarization mechanism commonly observed in ferrite materials. The $CoFe_2O_4$ sample exhibits the highest $\varepsilon'$and ε''values, indicating stronger polarization and dielectric loss behavior due to electron hopping between Fe^{2+}/Fe^{3+} ions. In contrast, $SrFe_{12}O_{19}$ exhibits the lowest values because of the high-resistivity of M-type hexaferrite. The R_m sample shows intermediate values between the two constituent phases, suggesting that the formation of interfaces between $SrFe_{12}O_{19}$ and $CoFe_2O_4$ enhances interfacial polarization and improves dielectric loss characteristics. The $SrFe_{12}O_{19}$ sample exhibits relatively low and stable μ'values, which are characteristic of magnetic materials with high magnetocrystalline anisotropy. In contrast, $CoFe_2O_4$ and the R_m samples show stronger fluctuations in μ', which are associated with natural ferromagnetic resonance and spin rotational processes in the microwave frequency region. Notably, the R_m samples exhibits the highest μ''values over most of the investigated frequency range, indicating enhanced magnetic loss capability due to exchange interactions between the hard magnetic $SrFe_{12}O_{19}$ phase and the soft magnetic $CoFe_2O_4$ phase. This enhanced magnetic loss behavior is highly beneficial for electromagnetic wave absorption applications and is consistent with previous reports on composite samples.

The dielectric ($\tan\delta_\varepsilon = \varepsilon''/\varepsilon'$) and magnetic loss tangent ($\tan\delta_\mu = \mu''/\mu'$) were determined. Figure 5 shows the dependence of $\tan\delta_\varepsilon$ and $\tan\delta_\mu$ on frequency (*f*). It can be observed that the $R_m$composite exhibits the highest $\tan\delta_\varepsilon$values over the entire investigated frequency range. This result indicates that the dielectric loss capability is significantly enhanced compared with those of the $SrFe_{12}O_{19}$ and $CoFe_2O_4$ samples. This behavior can be attributed to multiphase polarization and electron hopping between Fe^{2+}/Fe^{3+} ions at the heterogeneous interfaces formed between $SrFe_{12}O_{19}$ and $CoFe_2O_4$. In contrast, $SrFe_{12}O_{19}$ exhibits the lowest dielectric loss tangent due to the high-resistivity nature of M-type hexaferrite. Regarding the magnetic loss tangent ($\tan\delta_\mu$), the $R_m$sample also exhibits significantly higher values than those of the $SrFe_{12}O_{19}$ and $CoFe_2O_4$ samples. The enhanced magnetic loss can be associated with natural ferromagnetic resonance, spin rotational relaxation, and exchange interactions between the $SrFe_{12}O_{19}$ and $CoFe_2O_4$ magnetic phases. Meanwhile, $CoFe_2O_4$ exhibits the lowest $\tan\delta_\mu$values over most of the investigated frequency range, whereas $SrFe_{12}O_{19}$ shows moderate magnetic loss characteristics. The simultaneous enhancement of dielectric and magnetic losses in the R_m composite demonstrates its superior microwave attenuation capability, which is highly beneficial for electromagnetic wave absorption applications.

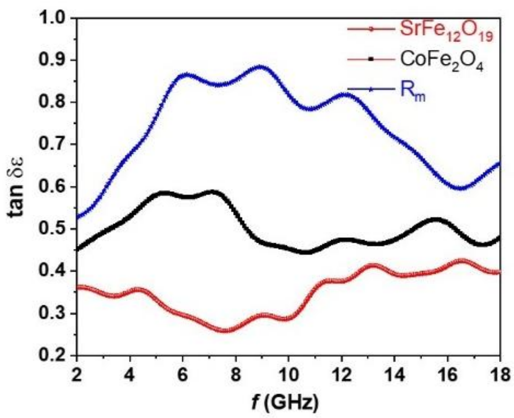

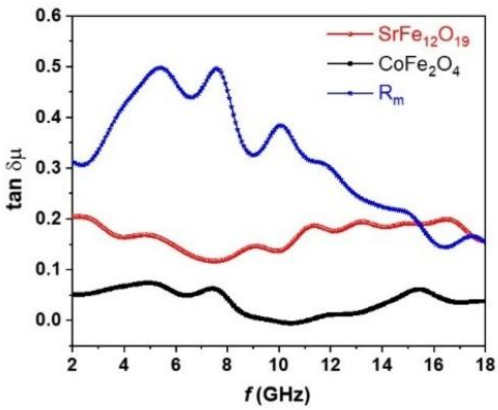

Figure 5. Frequency dependence of the dielectric ($\tan\delta_\varepsilon = \varepsilon''/\varepsilon'$) and magnetic loss tangent ($\tan\delta_\mu = \mu''/\mu'$).

Figure 6 shows the reflection loss (RL) curves of $SrFe_{12}O_{19}$, $CoFe_2O_4$, and the $R_m$composite with different absorber thicknesses in the frequency range of 2–18 GHz. It can be observed that the microwave absorption performance strongly depends on both the material composition and absorber thickness. In general, the absorption peaks shift toward lower frequencies with increasing thickness, which is consistent with the quarter-wavelength matching model commonly reported for microwave absorbing materials [7].

Among the investigated samples, $SrFe_{12}O_{19}$ exhibits excellent microwave absorption performance, with a minimum reflection loss (RL_{min}) of approximately −39 dB at around 11 GHz for a thickness of 2.5 mm. The $CoFe_2O_4$ sample shows relatively weaker absorption capability, with the strongest absorption peak reaching about −29 dB at approximately 14.5 GHz for the 3 mm sample. In contrast, the R_m composite demonstrates the best microwave absorption performance among all investigated samples. The composite achieves an RL_{min} value of approximately −43.4 dB at around 17 GHz with a thickness of 3 mm, indicating superior microwave attenuation capability.

Moreover, all samples exhibit RL values below −10 dB within certain frequency ranges, corresponding to more than 90% absorption of incident electromagnetic waves. Notably, the R_m composite presents broader effective absorption bandwidths compared with the individual $SrFe_{12}O_{19}$ and $CoFe_2O_4$ phases, suggesting improved impedance matching and enhanced attenuation characteristics. The enhanced microwave absorption performance of the composite can be attributed to the synergistic contribution of dielectric loss and magnetic loss, as well as interfacial polarization and exchange coupling interactions between the hard magnetic $SrFe_{12}O_{19}$ phase and the soft magnetic $CoFe_2O_4$ phase [20, 21]. The strong RL performance observed in this work is comparable to or better than many previously reported ferrite-based microwave absorbers. Similar enhancement mechanisms have been reported in hard/soft ferrite composites, where the coexistence of multiple dielectric and magnetic loss mechanisms contributes significantly to improved electromagnetic wave attenuation and impedance matching behavior. Therefore, the obtained results indicate that the prepared R_m composite is a promising candidate for high- performance electromagnetic wave absorption applications in the GHz frequency region.

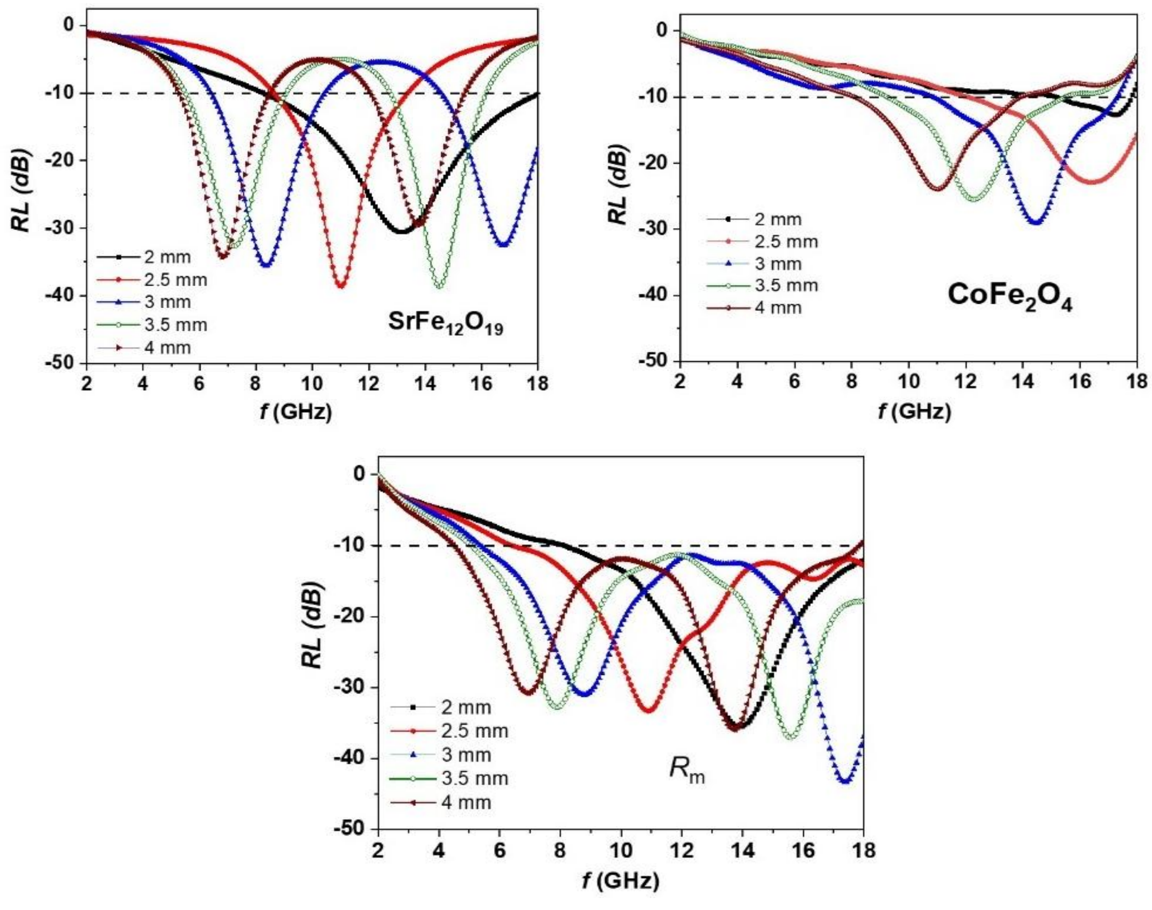

Figure 6. The reflection losses of $SrFe_{12}O_{19}$, $CoFe_2O_4$ and R_m samples.

4. Conclusion

The $SrFe_{12}O_{19}$, $CoFe_2O_4$, and $SrFe_{12}O_{19}/CoFe_2O_4$ samples were synthesised. Their microwave absorption properties were studied and compared in the 2–18 GHz range. Among the investigated samples, the $R_m$composite demonstrated the best microwave absorption performance, achieving a minimum reflection loss (RL_{min}) of approximately −43 dB at around 17 GHz with a thickness of 3 mm. In addition, the composite exhibited a broad effective absorption bandwidth with RL values below −10 dB over a wide frequency range, corresponding to more than 90% absorption of incident electromagnetic waves. The enhanced absorption performance was mainly attributed to the synergistic effect of dielectric loss, magnetic loss, interfacial polarization, natural ferromagnetic resonance, and exchange interactions between $SrFe_{12}O_{19}$ and $CoFe_2O_4$. These findings demonstrate that the prepared $SrFe_{12}O_{19}/CoFe_2O_4$ composite is a promising candidate for high-performance electromagnetic wave absorption applications in the GHz frequency region.

Acknowledgments

This research is funded by Hanoi University of Science and Technology (HUST) under project number T2024-TĐ-008.

References

[1] S. Mallesh, W. Jang, K. H. Kim, Facile Synthesis of Cube-Like Fe_3O_4-graphene Oxide Nanocomposites with Excellent Microwave Absorption Performance, Physics Letters, Section A: General, Atomic and Solid State Physics, Vol. 389, 2021, pp. 127069, https//doi.org/ 10.1016/j.physleta.2020.127069.

[2] E. Handoko1, S. Budi, I. Sugihartono, M. A. Marpaung, Z. Jalil, A.Taufiq, M. Alaydrus, Microwave Absorption Performance of Barium Hexaferrite Multi-Nanolayers, Materials Express, Vol. 10, No. 8, 2020, pp. 1328-1336, https//doi.org/10.1166/mex.2020.1811.

[3] A. Garg, S. Goel, N. Kumari, P. Soni, H. B. Baskey, S. Tyagi, Yttrium-doped Strontium Hexaferrite Particles for Microwave Absorption Application in X-band, Journal of Materials Science: Materials in Electronics, Vol. 31, No. 16, 2020, pp. 13746-13755, https//doi.org/10.1007/s10854-020-03934-2.

[4] S. Goel, A. Garg, R. K. Gupta, A. Dubey, N. E. Prasad, S. Tyagi, Development of $RGO/BaFe_{12}O_{19}$-based Composite Medium for Improved Microwave Absorption Applications, Appl. Phys. A Mater. Sci. Process., Vol. 126, No. 6, 2020, pp. 1-11, https//doi.org/10.1007/s00339-020-03613-3.

[5] H. Lv, Y. Guo, G. Wu, G. Ji, Y. Zhao, Z. J. Xu, Interface Polarization Strategy to Solve Electromagnetic Wave Interference Issue, Vol. 9, No. 6, 2017, https//doi.org/10.1021/acsami.6b16223.

[6] C. Pahwa, S. B. Narang, P. Sharma, Composition Dependent Magnetic and Microwave Properties of Exchange-Coupled Hard/Soft Nanocomposite Ferrite, J. Alloys Compd., Vol. 815, 2020, pp. 152391, https//doi.org/10.1016/j.jallcom.2019.152391.

[7] R. C. Pullar, Hexagonal Ferrites: A Review of the Synthesis, Properties and Applications of Hexaferrite Ceramics, Prog. Mater. Sci., Vol. 57, No. 7, 2012, pp. 1191-1334, https//doi.org/10.1016/j.pmatsci.2012.04.001.

[8] W. Chen, Q. Liu, X. Zhu, M. Fu, One-step in Situ Synthesis of Strontium Ferrites and Strontium Ferrites/Graphene Composites as Microwave Absorbing Materials, RSC Adv., Vol. 7, No. 64, 2017, pp. 40650-40657, https//doi.org/10.1039/c7ra05700h.

[9] S. V. Trukhanov, A. V. Trukhanov, V. G. Kostishyn, L. V. Panina, A. V. Trukhanov,V. A. Turchenko, D. I. Tishkevich, E. L. Trukhanova, Investigation into the Structural Features and Microwave Absorption of Doped Barium Hexaferrites, Dalton Transactions, Vol. 46, No. 28, 2017, pp. 9010-9021, https//doi.org/10.1039/c7dt01708a.

[10] S. Jiao et al., RGO/$BaFe_{12}O_{19}$/Fe_3O_4 Nanocomposite as Microwave Absorbent with Lamellar Structures and Improved Polarization Interfaces, Mater. Res. Bull., Vol. 108, 2018, pp. 89-95, https//doi.org/10.1016/j.materresbull.2018.08.014.

[11] S. Ren et al., Magnetoelectric Characterisation of $SrFe_{12}O_{19}$@MoS_2 Composites with High Microwave Absorption Performance, Ceram. Int., Vol. 51, No. 8, 2025, pp. 10184-10192, https//doi.org/10.1016/j.ceramint.2024.12.449.

[12] Q. Han, X. Meng, C. Lu, Exchange-coupled Ni0.5Zn0.5Fe_2O_4/$SrFe_{12}O_{19}$ Composites with Enhanced Microwave Absorption Performance, J. Alloys Compd., Vol. 768, No. 3, 2018, pp. 742-749, https//doi.org/ 10.1016/j.jallcom.2018.07.310.

[13] A. Houbi, Z. A. Aldashevich, Y. Atassi, Z. Bagasharova Telmanovna, M. Saule, K. Kubanych, Microwave Absorbing Properties of Ferrites and their Composites: A Review, J. Magn. Magn. Mater., Vol. 529, 2021, pp. 167839, https//doi.org/10.1016/j.jmmm.2021.167839.

[14] V. Bilovol, M. Sikora, K. Berent, Exchange Coupling in $SrFe_{12}O_{19}$/$CoFe_2O_4$ Composites: Effect of Component Proportions, J. Magn. Magn. Mater., Vol. 568, 2023, pp. 170384, https//doi.org/10.1016/j.jmmm.2023.170384.

[15] J. Chen, Z. Guo, Y. Tang, X. Zhang, Preparation and Microwave Absorption Properties of ZnO@Fe_3O_4 @RGO Composites, Physical Chemistry Chemical Physics, Vol. 27, No. 17, 2025, pp. 8960-8975, https//doi.org/10.1039/D5CP00636H.

[16] F. Jamadi, J. S. Yazdi, F. E. Tazangi, S. M. Hosseiny, The Impact of RGO and MWCNT/RGO on the Microwave Absorption of $NiFe_2O_4$@Fe_3O_4 in the Presence or Absence of PANI, J. Mater. Chem. A Mater., Vol. 12, No. 47, 2024, pp. 32981-3002, https//doi.org/10.1039/D4TA04128C.

[17] H. F. Lu, R. Y. Hong, H. Z. Li, Influence of Surfactants on Co-precipitation Synthesis of Strontium Ferrite, J. Alloys Compd., Vol. 509, No. 41, 2011, pp. 10127-10131, https//doi.org/10.1016/j.jallcom.2011.08.058.

[18] T. Thi, V. Nga, N. Thi, Fabrication and Exchange-Spring Properties of $SrFe_{12}O_{19}$@Fe_3O_4 Nanocomposites uith Core-shell Structure, Vol. 251, 2020.

[19] T. T. V. Nga, N. T. Lan, Fabrication and Exchange-spring Properties of $SrFe_{12}O_{19}$@Fe_3O_4 Nanocomposites with Core-Shell Structure, Mater. Chem. Phys., Vol. 251, 2020, pp. 123084, https//doi.org/10.1016/j.matchemphys.2020.123084.

[20] X. Huang, J. Zhang, Z. Liu, T. Sang, B. Song, H. Zhu, C. Wong, Facile Preparation and Microwave Absorption Properties of Porous Hollow $BaFe_{12}O_{19}$/$CoFe_2O_4$ Composite Microrods, J. Alloys Compd., Vol. 648, 2015, pp. 1072-1075, https//doi.org/10.1016/j.jallcom.2015.07.073.

[21] H. Yang, T. Ye, Y. Lin, J. Zhu, F. Wang, Microwave Absorbing Properties of the Ferrite Composites Based on Graphene, J. Alloys Compd., Vol. 683, 2016, pp. 567-574, https//doi.org/10.1016/j.jallcom.2016.05.127.